Surface Turbulent Heat and Momentum Fluxes over Global Oceans Based on the Goddard Satellite Retrievals, Version 2 (GSSTF2)

SHU-HSIEN CHOU

Laboratory for Atmospheres, NASA Goddard Space Flight Center, Greenbelt, Maryland

ERIC NELKIN

Science Systems and Applications, Inc., Lanham, Maryland

JOE ARDIZZONE

Science Applications International Corporation, Laurel, Maryland

ROBERT M. ATLAS

Laboratory for Atmospheres, NASA Goddard Space Flight Center, Greenbelt, Maryland

CHUNG-LIN SHIE

UMBC/Goddard Earth and Sciences Technology Center, NASA Goddard Space Flight Center, Greenbelt, Maryland

(Manuscript received 25 October 2002, in final form 28 March 2003)

ABSTRACT

Information on the turbulent fluxes of momentum, latent heat, and sensible heat at the air–sea interface is essential in improving model simulations of climate variations and in climate studies. A 13.5-yr (July 1987–December 2000) dataset of daily surface turbulent fluxes over global oceans has been derived from the Special Sensor Microwave Imager (SSM/I) radiance measurements. This dataset, Goddard Satellite-based Surface Turbulent Fluxes, version 2 (GSSTF2), has a spatial resolution of $1^\circ \times 1^\circ$ latitude–longitude and a temporal resolution of 1 day. Turbulent fluxes are derived from the SSM/I surface winds and surface air humidity, as well as the 2-m air and sea surface temperatures (SST) of the NCEP–NCAR reanalysis, using a bulk aerodynamic algorithm based on the surface layer similarity theory.

The GSSTF2 bulk flux model is validated by comparing hourly turbulent fluxes computed from ship data using the model with those observed fluxes of 10 field experiments over the tropical and midlatitude oceans during 1991–99. In addition, the GSSTF2 daily wind stress, latent heat flux, wind speed, surface air humidity, and SST compare reasonably well with those of the collocated measurements of the field experiments. The global distributions of 1988–2000 annual- and seasonal-mean turbulent fluxes show reasonable patterns related to the atmospheric general circulation and seasonal variations. Zonal averages of latent heat fluxes and input parameters over global oceans during 1992–93 have been compared among several flux datasets: GSSTF1 (version 1), GSSTF2, the Hamburg Ocean–Atmosphere Parameters and Fluxes from Satellite Data (HOAPS), NCEP–NCAR reanalysis, and one based on the Comprehensive Ocean–Atmosphere Data Set (COADS). Significant differences are found among the five. These analyses suggest that the GSSTF2 latent heat flux, surface air humidity, and winds are likely to be more realistic than the other four flux datasets examined, although those of GSSTF2 are still subject to regional biases. The GSSTF2 is useful for climate studies and has been submitted to the sea surface turbulent flux project (SEAFLUX) for intercomparison studies.

1. Introduction

The earth climate is a coupled system involving the ocean, land, and atmosphere. Information on the turbulent, radiative, and freshwater fluxes at the air–sea interface is essential in understanding the interaction between the atmosphere and oceans and in improving model simulations of climate variations. These fluxes are required for driving ocean models and validating coupled ocean–atmosphere global models. Surface measurements of these fluxes are scarce in both space and time. The Comprehensive Ocean–Atmosphere Data Set (COADS) has collected the most complete surface ma-

Corresponding author address: Dr. Shu-Hsien Chou, Laboratory for Atmospheres, NASA Goddard Space Flight Center, Code 912, Greenbelt, MD 20771.
E-mail: Shu-Hsien.Chou-1@nasa.gov

rine observations since 1854, mainly from merchant ships (Woodruff et al. 1993). However, the air–sea fluxes and input variables based on COADS have serious spatial and temporal sampling problems plus measurement uncertainty (e.g., da Silva et al. 1994; Josey et al. 1999; Wang and McPhaden 2001). Therefore, it is desirable that long-term global datasets of these fluxes be derived either from satellite observations or general circulation models (GCMs). A sea surface turbulent flux project (SEAFLUX; Curry et al. 2003, manuscripted submitted to *Bull. Amer. Meteor. Soc.*, hereafter C03) has been established to conduct intercomparison studies of ocean surface turbulent fluxes (momentum, latent heat, and sensible heat), flux models, and input parameters used for the derivation of turbulent fluxes.

Several efforts are under way to prepare datasets of ocean surface turbulent fluxes from satellite observations using bulk flux models (C03, and references therein). The Special Sensor Microwave Imager (SSM/I) on board a series of Defense Meteorological Satellite Program (DMSP) spacecraft has provided global radiance measurements for sensing the atmosphere and the surface. A number of techniques have been developed to derive the turbulent fluxes using parameters such as the surface air humidity and winds inferred from the SSM/I radiances (e.g., Chou et al. 1997; Schulz et al. 1997; Curry et al. 1999; Kubota et al. 2002).

Currently, there are several global datasets of ocean surface turbulent fluxes available, which are based on the SSM/I-retrieved surface air humidity and winds. The Hamburg Ocean–Atmosphere Parameters and Fluxes from Satellite Data (HOAPS) has provided pentad and monthly turbulent heat fluxes over global oceans with 1° spatial resolution for the period July 1987–December 1998, based on the method of Schulz et al. (1997). The Goddard Satellite-based Surface Turbulent Fluxes (GSSTF) dataset has two versions of global flux products derived from the SSM/I radiances. Version 1 (GSSTF1) has daily and monthly fields for July 1987–December 1994 with a spatial resolution of 2.0° × 2.5° latitude–longitude (Chou et al. 1997, 2000). Version 2 (GSSTF2) has daily and monthly fields for July 1987–December 2000 with 1° resolution, based on the method of Chou et al. (1997) with some improvements. The Japanese Ocean Flux Dataset with Use of Remote Sensing Observations (J-OFURO) has provided monthly turbulent heat fluxes over global oceans with 1° resolution for 1991–95 (Kubota et al. 2002). These four, along with other flux datasets, have been distributed to the SEAFLUX Web site for intercomparison studies (C03).

The satellite-retrieved air–sea fluxes and input parameters are subject to retrieval errors. On the other hand, errors in the surface fluxes and input parameters of GCMs can arise from the imperfect parameterization of physical processes, especially the boundary layer processes (e.g., Weller and Anderson 1996; Wang and McPhaden 2001; Smith et al. 2001; Renfrew et al. 2002). The scientists at the National Oceanic and Atmospheric Administration/Environmental Technology Laboratory (NOAA/ETL) have conducted several field experiments to provide high-quality data of surface meteorology and air–sea fluxes over the oceans using research ships (e.g., Fairall et al. 1996b, 1997, 2003). These data are very valuable for the validation of satellite retrievals and GCM products.

TABLE 1. Approximate local times (LT) of equatorial crossing and data records for each SSM/I of the DMSP satellites used in the derivation of GSSTF2.

Satellites	Equatorial crossing (LT)	Data records
F08	0615/1815	9 Jul 1987–31 Dec 1991
F10	0945/2145	1 Jan 1991–14 Nov 1997
F11	0600/1800	1 Jan 1992–31 Dec 1996
F13	0600/1800	3 May 1995–31 Dec 2000
F14	0845/2045	8 May 1997–31 Dec 2000

The purpose of this paper is to present an assessment of GSSTF2, which is one of the SEAFLUX activities. Section 2 describes the data sources used in this study. Section 3 briefly discusses the GSSTF2 bulk flux model and validation using hourly measurements of turbulent fluxes and input parameters of 10 field experiments conducted by the NOAA/ETL research ships over the tropical and midlatitude oceans during 1991–99 (Fairall et al. 2003; Brunke et al. 2003). Section 4 discusses the methodology for the satellite retrieval of daily turbulent fluxes, as well as the collocation validation of daily input parameters and turbulent fluxes of GSSTF2 against daily measurements of nine NOAA/ETL field experiments. Section 5 presents the spatial distributions of the GSSTF2 annual- and seasonal-mean turbulent fluxes and input parameters averaged over 1988–2000. Section 6 compares zonal averages of latent heat fluxes and input parameters over global oceans during 1992–93 for GSSTF1, GSSTF2, HOAPS, the National Centers for Environmental Prediction–National Center for Atmospheric Research (NCEP–NCAR) reanalysis (Kalnay et al. 1996), and da Silva et al. (1994). Concluding remarks are given in section 7.

2. Data sources

To derive GSSTF2 daily turbulent fluxes, the version-4 SSM/I surface (10-m) wind speeds and total precipitable water, and SSM/I antenna temperatures of Wentz (1997), as well as the sea surface temperature (SST), 2-m air temperature and sea level pressure of the NCEP–NCAR reanalysis, are used. The DMSP satellites pertinent to this study are *F8, F10, F11, F13,* and *F14,* which are polar orbiting with a period of ~102 min. Table 1 shows the approximate local times of equatorial crossing and data records for each of these satellites. Since January 1991, the earth system has been sensed by at least two SSM/Is with enhanced spatial and temporal coverage. Each satellite had a swath of 1394 km

TABLE 2. Times and locations of 10 field experiments conducted by the NOAA/ETL research ships.

Experiments	Times	Locations
ASTEX	6–28 Jun 1992	30°N, 36°W
COARE	11 Nov 1992–16 Feb 1993	1.7°S, 156°E
FASTEX	22 Dec 1996–26 Jan 1997	42°–52°N, 5°–60°W
JASMINE	4–31 May 1999	5°S–13°N, 88°–98°E
KWAJEX	28 Jul–10 Sep 1999	9°N, 167°E
MOORINGS	14 Sep–21 Oct 1999	8°N, 167°E–49°N, 130°W
NAURU99	15 Jun–18 Jul 1999	12°S, 130°E–8°N, 167°E
PACSF99	2 Nov–1 Dec 1999	8°S–12°N, 95°–121°W
SCOPE	17–28 Sep 1993	33°N, 118°W
TIWE	21 Nov–13 Dec 1991	0°, 140°W

on the earth surface. The SSM/I-retrieved surface winds and water vapor amounts have an original spatial resolution of $(25\ \text{km})^2$. They are averaged to daily values over $1^\circ \times 1^\circ$ latitude–longitude regions using data from all available DMSP satellites.

To validate GSSTF2 and the flux model, hourly measurements of surface meteorology and turbulent fluxes of 10 field experiments conducted by the NOAA/ETL research ships over the tropical and midlatitude oceans during 1991–99 are used (Fairall et al. 1997, 2003; Brunke et al. 2003). Table 2 shows the periods and locations of these 10 experiments: the Atlantic Stratocumulus Transition Experiment (ASTEX), the Coupled Ocean–Atmosphere Response Experiment (COARE), the Fronts and Atlantic Storm Track Experiment (FASTEX), the Joint Air–Sea Monsoon Interaction Experiment (JASMINE), the Kwajalein Experiment (KWAJEX), the Nauru '99 (NAURU99), the San Clemente Ocean Probing Experiment (SCOPE), the Tropical Instability Wave Experiment (TIWE), the Pan–American Climate Study in the eastern Pacific during 1999 (PACSF99), and the buoy service in the North Pacific (MOORINGS). These experiments provide hourly (50 min) covariance latent heat flux (LHF) and sensible heat flux (SHF) derived using the covariance or eddy correlation method. They also provide hourly wind stresses computed using the inertial-dissipation (ID) method. The wind stress determined by the ID method is more accurate than that derived using the covariance method for ship measurements (Fairall et al. 1996b, 2003). To reduce the flow distortion effects, only the data with the relative wind direction within 30° of the bow are used, except for SCOPE (Yelland et al. 1998). For SCOPE, data with wind directions 60°–100° relative to the bow are excluded. In addition, the latent heat fluxes and input parameters of GSSTF1, HOAPS, NCEP–NCAR reanalysis, and da Silva et al. (1994) over global oceans for the period 1992–93 are used to compare with those of GSSTF2.

3. GSSTF2 bulk flux model and validation

a. Bulk flux model

Recently, there have been extensive studies to develop and intercompare bulk flux algorithms (e.g., Chou 1993; Fairall et al. 1996b, 2003; Clayson et al. 1996; Bourassa et al. 1999; Zeng et al. 1998; Brunke et al. 2003). The GSSTF2 flux model is essentially the same as that of GSSTF1 (Chou et al. 1997; Chou 1993) except for two modifications. Chou (1993) developed the GSSTF1 flux model based on aircraft-observed covariance turbulent fluxes during cold air outbreaks over the northwestern Atlantic Ocean and provided a detailed discussion for the model. Thus, we first briefly describe the important common features of both models and then discuss the differences.

The wind stress (τ), SHF, and LHF are derived from the scaling parameters for wind or friction velocity (u_*), temperature (θ_*), and humidity (q_*) as

$$\tau = \rho u_*^2, \tag{1}$$

$$\text{SHF} = -\rho C_p u_* \theta_*, \tag{2}$$

$$\text{LHF} = -\rho L_v u_* q_*, \tag{3}$$

where ρ is air density, C_p the isobaric specific heat, and L_v the latent heat of vaporization. For a given SST and wind, temperature, and humidity at the measurement or reference heights within the atmospheric surface layer, the scaling parameters are solved through the roughness lengths and dimensionless gradients of wind, temperature, and humidity. The dimensionless gradients of wind (ϕ_u), potential temperature (ϕ_t), and humidity (ϕ_q) are functions of the stability parameter z/L, where z is the measurement height, and L the Monin–Obukhov length, which depends on the scaling parameters or fluxes. For the stable situation they are given as (Large and Pond 1982)

$$\phi_u = \phi_t = \phi_q = 1 + 7z/L. \tag{4}$$

For the unstable situation, they are given as (Businger et al. 1971)

$$\phi_u = (1 - 16z/L)^{-1/4}, \tag{5}$$

$$\phi_t = \phi_q = (1 - 16z/L)^{-1/2}. \tag{6}$$

The roughness lengths for wind (z_o), temperature (z_{ot}), and humidity (z_{oq}) are parameterized as (Charnock 1955; Garratt 1977; Liu et al. 1979)

$$z_o = 0.0144u_*^2/g + 0.11\nu/u_*, \quad (7)$$

$$z_{ot} = \nu/u_*(a_1 \mathrm{Rr}^{b_1}), \quad (8)$$

$$z_{oq} = \nu/u_*(a_2 \mathrm{Rr}^{b_2}), \quad (9)$$

where g is the gravitational acceleration, ν the kinematic viscosity of air, Rr ($=z_o u_*/\nu$) the roughness Reynolds number, and a_1, a_2, b_1, and b_2 the coefficients that depend on Rr and are taken from Liu et al. (1979). Note that the roughness lengths z_{ot} and z_{oq} are essentially the same as those of the COARE algorithm (version 2.5; Fairall et al. 1996b). However, the coefficient of the first term of z_o (7), which is generally referred to as the Charnock parameter (α) and is adopted according to Garratt (1977), is slightly larger than that of the COARE algorithm (0.0144 versus 0.011). Note that Yelland and Taylor (1996) found that α increased from 0.011 to 0.017 as winds increase from 6 to 26 m s^{-1}. Fairall et al. (2003) have modified α to have wind speed dependency. There are some studies suggesting that z_o should depend on ocean wave age and/or wave slope (e.g., Taylor and Yelland 2001; Oost et al. 2002; Bourassa et al. 1999). However, the wave information is not yet available for the flux retrieval over global oceans.

The LHF and SHF depend on the skin SST. The skin SST is generally cooler than the bulk SST with a daily mean difference of ~0.2°C, but its instantaneous value relies on various bulk-skin SST difference models, surface net heat flux, and wind-induced oceanic mixing (e.g., Fairall et al. 1996a; Webster et al. 1996; Wick et al. 1996; C03). The global distribution of skin SST is not currently available. To partially compensate for the cool skin effect on LHF, the GSSTF1 flux model estimates the saturation specific humidity at the sea surface (Q_s) using the approximated formulation as $Q_s = (0.622e/P)$. Here e is the saturation vapor pressure for pure water at the bulk SST, and P is the sea level pressure. On the other hand, the cool skin effect on SHF is not considered.

There are two differences between the GSSTF1 and GSSTF2 bulk flux models. The first difference is related to the salinity effect on Q_s. The GSSTF1 model ignores this effect and sets $Q_s = (0.622e/P)$, while the GSSTF2 model includes the salinity effect and sets $Q_s = 0.98(0.622e/P)$. This is because the saturation vapor pressure is ~2% smaller for saline water than for pure water (Fairall et al. 1996b; Zeng et al. 1998). The second difference is related to the assumptions of the von Karman constants. The GSSTF1 model adopts different von Kármán constants of 0.4, 0.36, and 0.45, for velocity, temperature, and humidity, respectively, which performs the best among the four bulk flux schemes tested for cold air outbreaks over the midlatitude ocean by Chou (1993). On the other hand, the GSSTF2 flux model assumes the identical von Kármán constant of 0.4 for the three variables following the recent studies over oceans (e.g., Fairall et al. 1996b, 1997, 2003; Zeng et al. 1998; Brunke et al. 2003, and references therein). The change in the von Kármán constants causes the GSSTF2 transfer coefficients to decrease 11% for LHF but to increase 11% for SHF, as compared to those of GSSTF1. These two changes in the flux model thus cause the LHF to be smaller for GSSTF2 than for GSSTF1, if the input parameters remain the same. The GSSTF2 neutral transfer coefficients (at 10-m height) for wind stress, SHF, and LHF are 1.02–1.81 $\times 10^{-3}$, 1.01–1.18 $\times 10^{-3}$, and 1.05–1.22 $\times 10^{-3}$, respectively, for the 10-m wind of 3–18 m s^{-1}. The coefficients increase with decreasing wind when 10-m winds are less than 3 m s^{-1}. The GSSTF2 transfer coefficients (for 10-m winds up to ~18 m s^{-1}) are in close agreement with those of Zeng et al. (1998), Fairall et al. (1996b), and Renfrew et al. (2002).

b. Validation of bulk flux model

To validate the flux model, hourly turbulent fluxes are computed from ship data using the GSSTF2 flux model. These ship data are hourly wind speed, specific humidity, and temperature of the surface air, and SST (at the 5-cm depth) of the 10 field experiments shown in Table 2. Table 3 compares the hourly ID wind stress, covariance LHF, and covariance SHF for each of the 10 experiments with those computed from ship data using the GSSTF2 bulk flux model. It can be seen from Table 3 that the turbulent fluxes measured during FASTEX are significantly larger than those of other experiments due to higher winds (reaching ~20 m s^{-1}). In addition, the surface turbulent fluxes measured during COARE have been intensively analyzed, and compared by numerous scientists (e.g., Fairall et al. 1996b; Weller and Anderson 1996; Chou et al. 1997, 2000; Schulz et al. 1997; Curry et al. 1999). It is interesting to know the comparison for these two experiments. Thus, we use different symbols for the scatterplot of Fig. 1: F for FASTEX, C for COARE, and X for other experiments.

It can be seen from Fig. 1 and Table 3 that the hourly wind stress and LHF computed using the GSSTF2 flux model agree very well with those of the observed. Compared to 1913 samples of hourly observed turbulent fluxes of the 10 experiments, the computed hourly wind stress has a negative bias of -0.0005 N m^{-2}, a standard deviation (SD) error of 0.0106 N m^{-2}, and a correlation of 0.98, with a correlation range of 0.91–0.99. The SD error is the standard deviation of the differences between the computed and observed. The computed hourly LHF has a bias of 4.5 W m^{-2}, an SD error of 19.6 W m^{-2}, and a correlation of 0.91, with a correlation range of 0.77–0.95. The computed hourly SHF has a negative bias of -0.2 W m^{-2}, an SD error of 7.3 W m^{-2}, and a correlation of 0.82, with a correlation range of 0.44–0.91. Note that the model–ship differences in hourly turbulent fluxes include errors in the parameterization of the GSSTF2 flux model, as well as the uncertainty in the input variables and fluxes measured by the ships (e.g., Fairall et al. 1996b). The computed SHF appears

TABLE 3. Comparison of hourly (50-min) ID wind stresses, covariance LHF, and covariance SHF for each of 10 field experiments with those computed from ship data using GSSTF2 bulk flux model. The mean is the average observed fluxes for N samples of the experiment, positive bias indicates larger computed fluxes, SDE is std dev error, and r is correlation coefficient. Units are 10^{-3} N m^{-2} for wind stress, and W m^{-2} for heat fluxes.

		Stress				LHF				SHF			
Experiment	N	Mean	Bias	SDE	r	Mean	Bias	SDE	r	Mean	Bias	SDE	r
ASTEX	109	47.8	−3.6	7.8	0.97	64.7	15.1	13.1	0.87	4.8	1.6	2.5	0.84
COARE	565	36.5	−1.0	6.1	0.99	103.3	2.6	21.3	0.89	7.5	−0.8	3.9	0.79
FASTEX	92	215	−4.7	33.9	0.98	150.9	−10.1	32.7	0.93	41.7	−13.6	25.2	0.77
JASMINE	121	36.4	−3.0	13.1	0.95	92.9	15.3	24.0	0.77	4.9	0.2	3.8	0.62
KWAJEX	451	32.6	2.5	5.8	0.97	92.9	3.0	14.9	0.84	5.4	1.1	3.3	0.57
MOORINGS	89	38.2	0.5	9.6	0.93	91.7	8.7	16.6	0.90	4.0	2.7	3.3	0.60
NAURU99	232	30.8	2.0	7.3	0.96	104.7	5.2	19.0	0.89	4.7	0.8	3.8	0.44
PACSF99	10	66.2	−6.1	10.0	0.96	115.1	−4.6	24.5	0.90	8.2	4.3	3.3	0.91
SCOPE	232	31.1	−2.9	7.1	0.98	48.1	5.2	10.7	0.95	13.7	0.8	4.7	0.85
TIWE	12	70.8	−9.5	9.9	0.91	117.5	1.7	16.8	0.85	0.8	2.7	2.7	0.56
All	1913	43.9	−0.5	10.6	0.98	93.4	4.5	19.6	0.91	8.5	−0.2	7.3	0.82

to have lower accuracy, compared to the computed wind stress and LHF. This is most likely due to the fact that the small SHF is more sensitive to measurement and parameterization errors, especially the diurnal variation of the cool skin effect. Overall the results suggest that the GSSTF2 flux model is generally accurate for weak and moderate winds, but slightly underestimates LHF and SHF for strong winds.

4. Methodology and validation for GSSTF2 daily retrievals

a. Methodology for GSSTF2 daily retrievals

The methods for deriving the GSSTF2 daily turbulent fluxes and input parameters essentially follow those of Chou et al. (1997). Thus, the key features of the methodology are briefly discussed in this section. Daily turbulent fluxes are derived using the GSSTF2 bulk flux model from daily mean values of the SSM/I 10-m wind speed (U_{10m}) of Wentz (1997) and SSM/I 10-m specific humidity (Q_{10m}), and 2-m air temperature (T_{2m}) and SST of NCEP–NCAR reanalysis (referred to as NCEP hereafter). The SSM/I senses the earth atmosphere system with seven channels at 19.3 (V, H), 22.2 (V), 37.0 (V, H), and 85.5 (V, H) GHz, where V and H indicate vertical and horizontal polarization, respectively. The Wentz (1997) algorithm simultaneously produces the SSM/I version-4 products for U_{10m}, vertically integrated water vapor (total precipitable water), columnar cloud water, and rain rate. It produced these four geophysical parameters by matching all the brightness temperatures of the five SSM/I low-frequency channels to those computed using a radiative transfer model of the atmosphere and ocean. The directions of wind stress are taken from those of the surface winds, which are derived from a blend of the Wentz (1997) SSM/I U_{10m}, surface wind vectors from ships, buoys, and NCEP following the method of Atlas et al. (1996).

The methodology for retrieving daily Q_{10m} follows that of Chou et al. (1995, 1997), who extended the approaches of Schulz et al. (1993) and Wagner et al. (1990). Schulz et al. (1993) retrieved instantaneous Q_{10m} from SSM/I using a linear Q_{10m}–W_B relation due to their high correlation of 0.96, where W_B is the bottom-layer (the lowest atmospheric 500-m layer) precipitable water. They retrieved W_B from the SSM/I brightness temperatures at 19.3 (V, H), 22.2 (V), and 37.0 (V) GHz, as these channels had the maximum weighting functions in the bottom layer. Wagner et al. (1990) found that the first two vertical empirical orthogonal functions (EOFs) of specific humidity soundings of a climatic regime based on regions were very useful for retrieving the instantaneous Q_{10m} over the North Atlantic Ocean. Chou et al. (1995, 1997) retrieved the instantaneous/daily Q_{10m} from the instantaneous/daily total precipitable water (W) and W_B using the first two vertical EOFs of First Global Atmospheric Research Programme (GARP) Global Experiment (FGGE) IIb humidity soundings of six W-based climatic regimes over global oceans during December 1978–November 1979. Daily W_B is derived from SSM/I following Schultz et al. (1993), while daily W is taken from that of Wentz (1997) for the GSSTF2.

The LHF and SHF depend on the skin SST. However, the SST of NCEP is derived by regressing the bulk SST against the satellite IR radiance measurements (Reynolds and Smith 1994). As mentioned above, the daily mean bulk SST is generally warmer than the skin SST by ~0.2°C with the difference depending on surface net heat flux and wind-induced oceanic mixing (Fairall et al. 1996b; Webster et al. 1996; Wick et al. 1996). The global distribution of skin SST for the period of interest is not currently available and is still under extensive study (C03). Thus we use the bulk SST of NCEP to compute heat fluxes. To use the GSSTF2 flux model or other bulk flux models to derive SHF, the measurements of air temperatures in the atmospheric surface layer (with a depth of ~50–100 m) are required. However, they are not currently available from satellite measurements. Thus, the daily mean T_{2m} used for computing SHF is taken from that of NCEP. Sea–air temperature

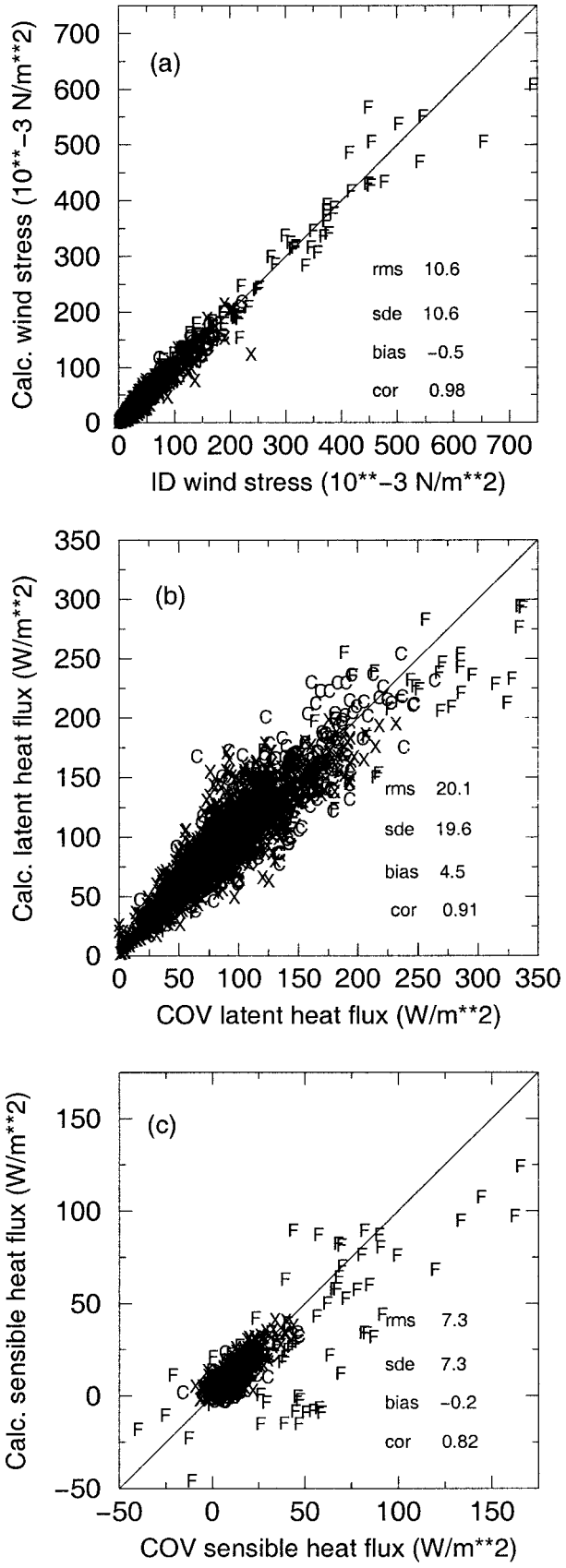

difference is generally very small over the open ocean, except for the western Pacific warm pool and midlatitudes in the winter. Small errors in the SSTs and air temperatures could induce a relatively large error in the sea–air temperature difference if the errors are uncorrelated. The T_{2m} of NCEP is thermodynamically constrained to the SST.

b. Collocation validation for GSSTF2 daily retrievals

Table 4 and Figs. 2 and 3 compare daily mean GSSTF2 turbulent fluxes and input parameters with those of the 10 field experiments of Table 2, except for SCOPE. Note that there are no data for GSSTF2 to collocate with SCOPE as it is too close to the coastline. The GSSTF2 daily wind speed (U), specific humidity (Q_a), and temperature (T_a) of the surface air are adjusted to the measurement heights of the ships (~14–21 m) for proper validation using the GSSTF2 flux model. The GSSTF2 daily SST is compared with the bulk SST at the 5-cm depth measured by the ships. The comparison with five major tropical experiments with large samples (ASTEX, COARE, JASMINE, NAURU99, and KWAJEX) is also shown in Table 4 for reference.

Table 4 shows that the GSSTF2 daily Q_a has a positive bias of ~1 g kg^{-1} in the tropical oceans, especially for $Q_a > 16$ g kg^{-1} (Fig. 3b). However, the LHF has a rather small negative bias of ~ -2.6 W m^{-2} in the tropical oceans. This is mainly due to the fact that, in the tropical oceans, the GSSTF2 flux model produces a small positive bias of ~5 W m^{-2} for LHF and the weak winds associated with moist air have a small positive bias of ~0.3 m s^{-1} (Tables 3 and 4). These two factors offset the underestimation of LHF due to a positive bias of humidity. On the other hand, the GSSTF2 SHF has a large positive bias of ~7 W m^{-2} in the tropical oceans. This mainly arises from the negative bias of T_a of NCEP, especially for $T_a > 26$°C (Fig. 3c), a fact that was also found by Smith et al. (2001), and Wang and McPhaden (2001). Some of the positive bias of SHF can also be caused by the use of bulk SST instead of skin SST.

Sources of retrieval–ship differences in daily turbulent fluxes and input parameters include the spatial–temporal mismatch between GSSTF2 and ships, as well as the errors in the input parameters and fluxes for both GSSTF2 and ship observations. The collocated daily GSSTF2 variables are computed from two to three satellite observations averaged over a 1° area that encloses the ship locations, while those of the ships are computed from at least 2-h measurements over a much smaller

←

FIG. 1. The 1913-hourly fluxes calculated from ship data using the GSSTF2 bulk flux model vs the observed (a) wind stresses determined by the ID method, and (b) latent and (c) sensible heat fluxes determined by the covariance or eddy correlation method of 10 field experiments. Here C is for COARE, F for FASTEX, and X for other experiments.

TABLE 4. Comparison of daily wind stress, LHF, SHF, surface wind speed (U), surface air humidity (Q_a) and temperature (T_a), and SST of GSSTF2 with those of all nine field experiments and five tropical experiments with large samples. The mean is ship-observed values averaged over collocated days, positive bias indicates larger GSSTF2, SD error is std dev of differences, and r is correlation coefficient. Units are 10^{-3} N m^{-2} for wind stress, W m^{-2} for heat fluxes, m s^{-1} for U, g kg^{-1} for Q_a, and °C for T_a and SST.

					SD error		
Source	Days	Variable	Mean	Bias	Daily	Monthly	r
All	167	stress	54.1	12.9	74.4	13.6	0.72
Tropics	134	sress	32.7	5.3	19.3	3.5	0.81
All	167	LHF	99.8	0.8	35.8	6.5	0.83
Tropics	134	LHF	93.0	−2.6	29.7	5.4	0.80
All	167	SHF	8.9	6.4	10.1	1.8	0.84
Tropics	134	SHF	5.5	7.0	6.2	1.1	0.45
All	240	U	5.9	0.36	1.38	0.25	0.92
Tropics	139	U	4.6	0.31	1.07	0.20	0.87
All	240	Q_a	15.7	0.67	1.23	0.22	0.97
Tropics	139	Q_a	17.7	1.01	1.11	0.20	0.85
All	240	T_a	24.6	−0.47	0.82	0.15	0.99
Tropics	139	T_a	27.2	−0.70	0.76	0.14	0.94
All	279	SST	25.7	0.04	0.51	0.09	1.00
Tropics	157	SST	28.4	0.02	0.30	0.05	0.99

area. Assuming daily retrieval errors are independent, Table 4 shows the SD errors for the monthly mean wind stress, LHF, and SHF reduce to 0.0136 (0.0035) N m^{-2}, 6.5 (5.4) W m^{-2}, and 1.8 (1.1) W m^{-2}, respectively, as inferred from the nine (five tropical) experiments. The SD errors for the monthly mean U, Q_a, T_a, and SST reduce to 0.25 (0.20) m s^{-1}, 0.22 (0.20) g kg^{-1}, 0.15°C (0.14°C), and 0.09°C (0.05°C), respectively, as inferred from the nine (five tropical) experiments.

5. 1988–2000 annual- and seasonal-mean air–sea turbulent fluxes

a. Annual means

Figure 4 shows spatial distributions of the GSSTF2 annual-mean U_{10m}, sea–air humidity difference ($Q_s - Q_{10m}$), and sea–air temperature difference (SST $- T_{2m}$) averaged over 1988–2000, respectively. Figure 5 shows the spatial distributions of the GSSTF2 annual-mean wind stress, LHF, and SHF averaged over the same 13-yr period, respectively. Figures 4a and 5a show that the maximum annual-mean wind speed and stress are located in the trade wind belts (~8–9 m s^{-1}, ~0.09–0.12 N m^{-2}) and extratropical storm track regions (~8–11 m s^{-1}, ~0.09–0.2 N m^{-2}). The minimum annual-mean wind speed and stress (<~0.03 N m^{-2}) are located in the weak wind (~4–6 m s^{-1}) areas of the intertropical convergence zone (ITCZ), South Pacific convergence zone (SPCZ), and tropical Indian Ocean, as well as the subtropical highs (~7 m s^{-1}). Figure 5b shows that the maximum LHF is located in the trade wind belts (~150–180 W m^{-2}) and in the western boundary current regions of Kuroshio and the Gulf Stream (~150 W m^{-2}). This results from high winds (~8–9 m s^{-1}) coupling with large $Q_s - Q_{10m}$ (~5–6 g kg^{-1}) in these areas (Figs. 4a and 4b). The minimum LHF (<~60 W m^{-2}) is found in the eastern equatorial Pacific and Atlantic, due to upwelling-induced cold SSTs associated with weak winds, and in the high latitudes due to the poleward decrease of SST. The SHF is generally very small (<~10–15 W m^{-2}) due to the smallness of SST $- T_{2m}$ (<~1°–1.5°C), except for slightly larger fluxes in the northwestern parts of the North Pacific and North Atlantic arising from cold air outbreaks (Figs. 4c and 5c). The spatial distributions of the GSSTF2 annual-mean LHF and input parameters averaged over 1988–2000 (Figs. 4 and 5) are similar to those of GSSTF1, HOAPS, J-OFURO, and NCEP (Kubota et al. 2003). However, there are quantitative differences among various global flux datasets, and these are discussed in section 6.

b. Seasonal means

The seasonal-mean wind stress and LHF along with the input parameters averaged over the four seasons of December–February (DJF), March–May (MAM), June–August (JJA), and September–November (SON) of 1988–2000 are discussed. Figures 6 and 7 show the spatial distributions of the GSSTF2 seasonal-mean U_{10m} and wind stress for the 1988–2000 four seasons, respectively. The maximum wind speed and stress are generally found in the trade wind zones, the tropical Indian Ocean (associated with the southwest summer monsoon circulation), the wintertime extratropical North Pacific and North Atlantic (associated with synoptic activities), and the Southern Hemisphere extratropical oceans. The wind speed and stress in the trade wind zones are larger in the Northern Hemisphere than in the Southern Hemisphere during DJF and MAM, and vice versa during the other two seasons, as a result of seasonal variations of the Hadley circulation. The minimum wind speed and stress are generally found in the tropical Indian Ocean and SPCZ during DJF and MAM, near Indochina during JJA and SON, the ITCZ in the

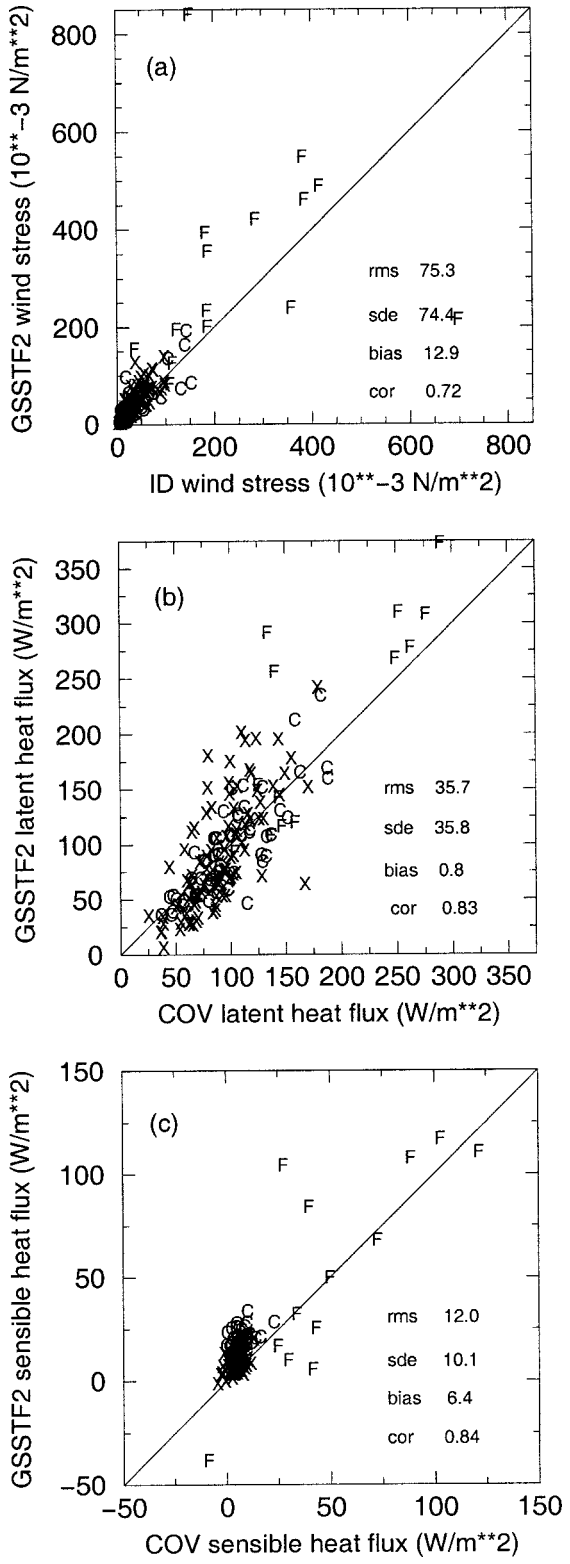

FIG. 2. GSSTF2 daily flux retrievals vs the observed (a) ID wind stresses, (b) covariance latent heat fluxes, and (c) covariance sensible heat fluxes of nine field experiments. The symbols are the same as in Fig. 1.

eastern equatorial Pacific and Atlantic, and the subtropical highs. The surface wind speed and stress fields, shown in Figs. 6 and 7, clearly demonstrate the seasonal variations of the atmospheric general circulation. The spatial distributions of seasonal-mean surface wind and stress are similar to those of GSSTF1 (Chou et al. 1997), Atlas et al. (1996), Esbensen et al. (1993), Chou et al. (1995), and Hellerman and Rosenstein (1983).

Figures 8 and 9 show spatial distributions of the GSSTF2 seasonal-mean $Q_s - Q_{10m}$ and LHF averaged over 1988–2000, respectively. The patterns of the seasonal-mean LHF follow more closely those of U_{10m} in the tropical oceans, but follow more closely those of $Q_s - Q_{10m}$ in the extratropical oceans and the equatorial eastern Pacific and Atlantic (Figs. 6, 8, and 9). All three variables are larger in the winter than in the summer hemisphere. The high LHF ($\sim$180–210 W m^{-2}) is generally found in the trade wind zones of both hemispheres, where strong U_{10m} of $\sim$8–10 m s^{-1} are associated with large $Q_s - Q_{10m}$ of $\sim$6–7 g kg^{-1}. The larger U_{10m}, $Q_s - Q_{10m}$, and LHF in the trade wind belt during the winter than during the summer are due to the stronger wintertime Hadley circulation (Figs. 6–9). In addition, the maximum LHF of $\sim$210–270 W m^{-2} is found in the Kuroshio and Gulf Stream areas (Fig. 9a). Strong U_{10m} of $\sim$10–12 m s^{-1} coupling with large $Q_s - Q_{10m}$ of $\sim$5–7 g kg^{-1} prevail in these regions during the winters (Figs. 6a and 8a). This results from the cold, dry continental air with strong offshore winds flowing over the warm oceans in the regions (e.g., Chou and Ferguson 1991; Chou 1993). The LHF and $Q_s - Q_{10m}$ decrease poleward with decreasing SST, with the minima located in high latitudes of the summer hemisphere. In the equatorial eastern Pacific and Atlantic for all seasons, the LHF and $Q_s - Q_{10m}$ are also found to decrease eastward with decreasing SST due to upwelling induced cold SST. The large-scale patterns and seasonal variations of the LHF are similar to those of GSSTF1, HOAPS, and J-OFURO (Chou et al. 1997; Schulz et al. 1997; Kubota et al. 2002, 2003).

6. Comparison of LHF with other datasets

The surface turbulent fluxes are derived using various bulk flux algorithms from surface winds, surface air humidity and temperature, and SST, all of which may have a large uncertainty in the reanalyses, satellite retrievals, and COADS. There is no ''ground truth'' for the global flux fields; thus the intercomparison studies are required to assess the sources of errors for various global flux products. The studies can identify the strengths and weaknesses of various flux products, and provide important information for improving atmospheric GCMs and satellite retrievals. As NCEP and da Silva et al. (1994, referred to as da Silva) have been widely used for various climate studies, it is important to include them for the comparison. Kubota et al. (2003) compared the 1992–94 LHF derived from GSSTF1,

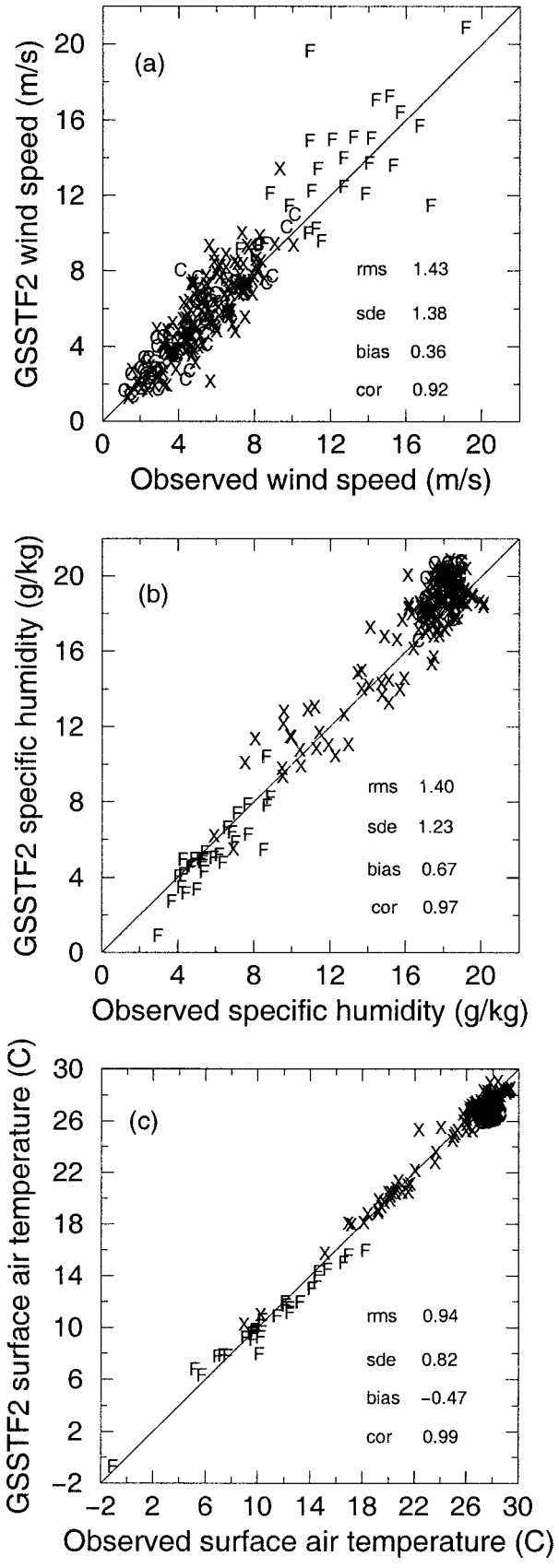

HOAPS, J-OFURO, NCEP, and the European Centre for Medium-Range Weather Forecasts (ECMWF) analysis, as well as the 1992–93 LHF of da Silva, over the global oceans. They found that the large-scale patterns of LHF are generally similar but with quantitative differences among various products. In this study we compare 1992–93 monthly LHF and input parameters among GSSTF1, GSSTF2, HOAPS, NCEP, and da Silva. To evaluate the differences among various flux products, only the space and time matched monthly mean valid data for the common period of 1992–93 are used for the comparison. Thus this study is different from Kubota et al. (2003).

Figure 10 shows zonal averages of the LHF, U_{10m}, and sea–air humidity difference ($Q_s - Q_a$) over global oceans during 1992–93 for GSSTF2, HOAPS, NCEP, and da Silva, respectively. Figure 11 shows zonal averages of the differences of HOAPS, NCEP, and da Silva from GSSTF2 for these parameters during the same period. The GSSTF2, HOAPS, and da Silva include a 2% reduction in Q_s related to the salinity effect, but NCEP does not. To properly compare U_{10m}, the 20-m wind speed of da Silva is multiplied by 0.94 to adjust to that at the 10-m height. The adjustment factor 0.94 is obtained by assuming a logarithmic wind profile with a wind roughness length of 1.52×10^{-4}, which is equivalent to a neutral drag coefficient of 1.3×10^{-3} at the 10-m height (Wentz 1997). Mears et al. (2001) found the effect of stability on the height adjustment for wind speeds to be insignificant. The Q_a is not adjusted. The reference heights of Q_a are 10 m for GSSTF2 and HOAPS, 2 m for NCEP, and 20 m for da Silva. The Q_a is generally larger at the 2-m height than at the 10-m height by $\sim$0.6 g kg^{-1} for $Q_s - Q_a$ of 5 g kg^{-1} and by $\sim$0.1 g kg^{-1} for $Q_s - Q_a$ of 1 g kg^{-1}. The humidity difference at the 10- and 20-m heights is generally negligible. Thus the different reference heights are not main causes for the differences of Q_a shown in Fig. 11c. Note that the results for GSSTF1 are not shown in Figs. 10 and 11. This is because the differences between GSSTF1 and GSSTF2 are generally negligibly small, except for the LHF. The LHF averaged over the oceans within 60°S–60°N (referred to as the global average) is 12.7 W m^{-2} larger for GSSTF1, as compared to GSSTF2. This difference ($\sim$12% of the global average LHF for GSSTF2) mainly arises from the different von Karman constant for humidity between GSSTF1 (0.45) and GSSTF2 (0.40) as discussed in section 3.

Figure 10a shows that the LHF, for the four flux products, has a maximum in the trade wind regions of both hemispheres and decreases equatorward and poleward, with the minimum near the equator and high latitudes.

←

FIG. 3. GSSTF2 daily (a) winds, (b) specific humidity, and (c) temperatures of surface air vs those of nine field experiments. The symbols are the same as in Fig. 1.

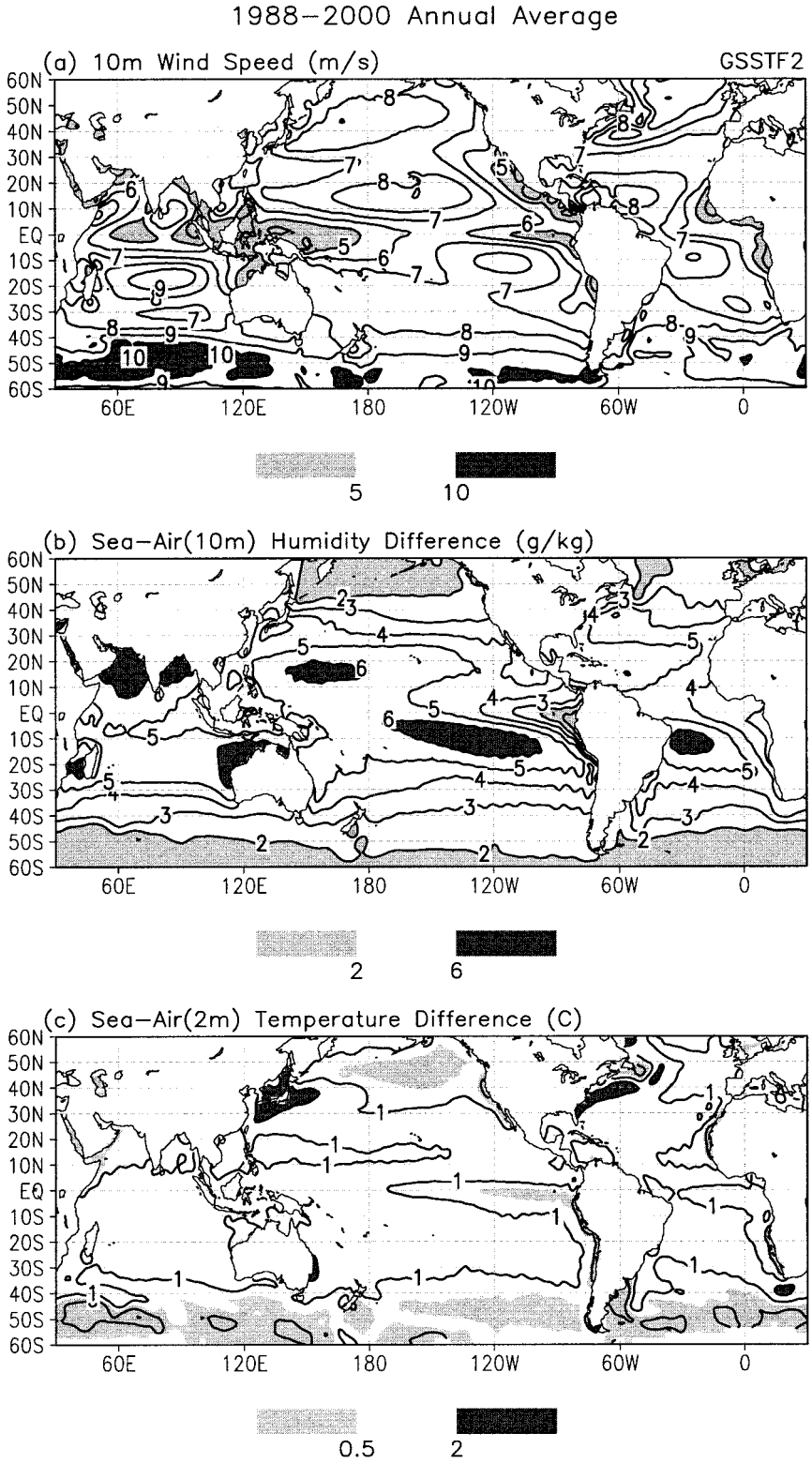

FIG. 4. Annual-mean (a) 10-m wind speed, (b) sea–10-m humidity difference, and (c) SST–2-m temperature difference averaged over 1988–2000 for GSSTF2.

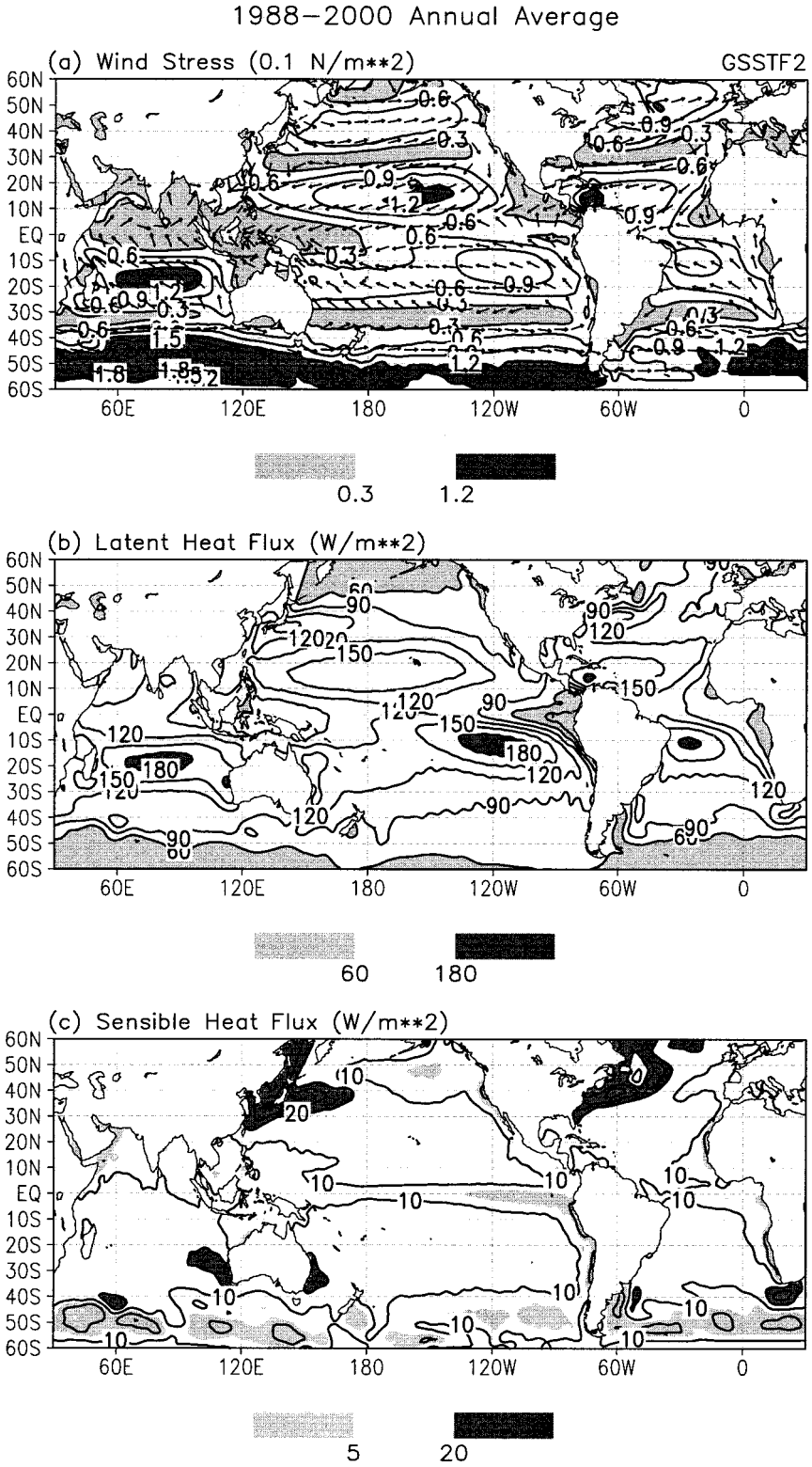

FIG. 5. Annual-mean (a) wind stress, (b) LHF, and (c) SHF averaged over 1988–2000 for GSSTF2. Arrows indicate wind stress directions.

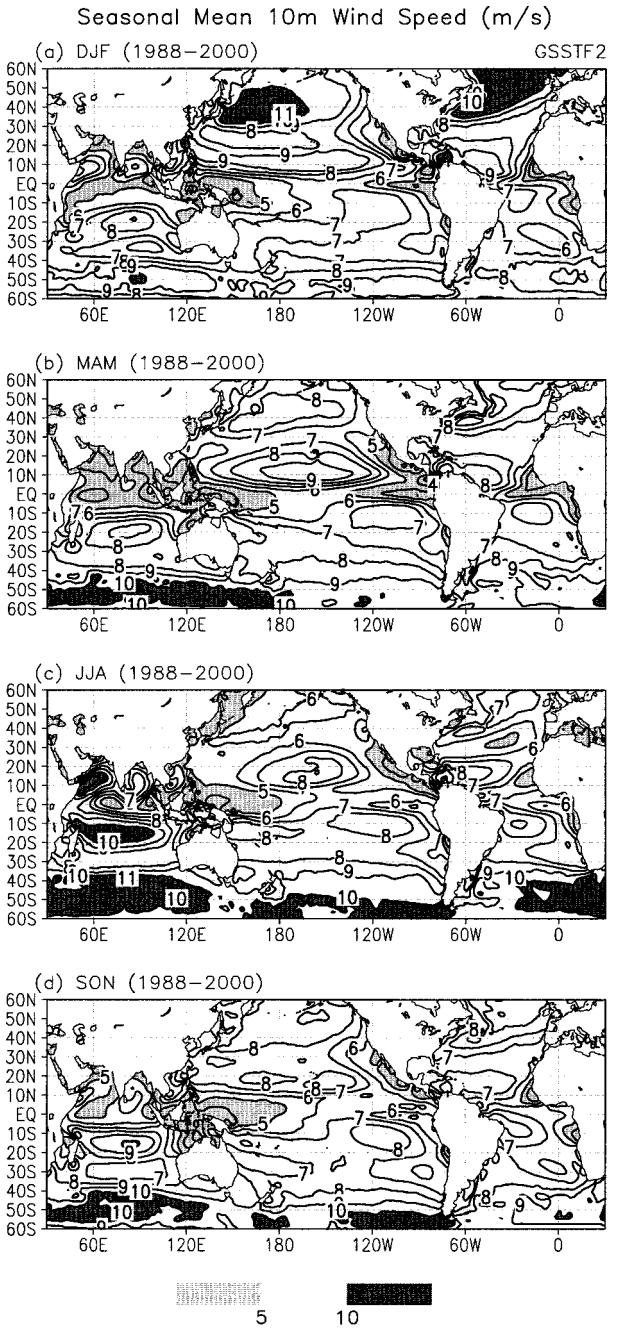

FIG. 6. Seasonal-mean 10-m wind speeds for (a) DJF, (b) MAM, (c) JJA, and (d) SON averaged over 1988–2000 for GSSTF2.

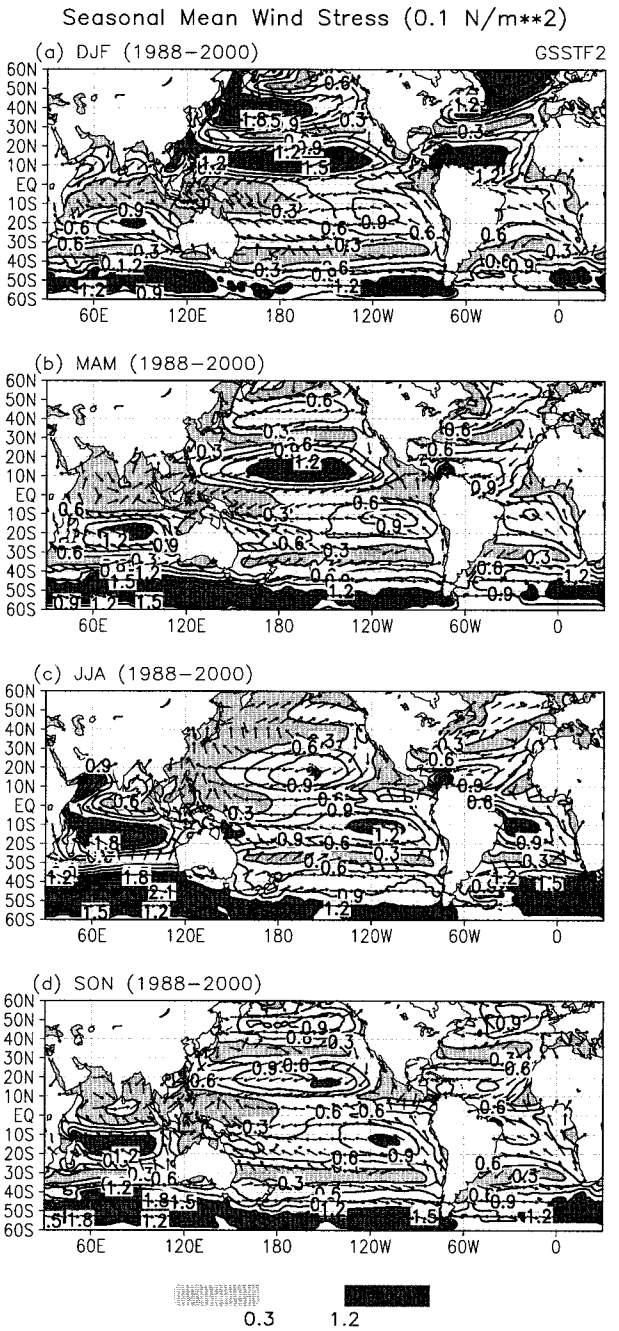

FIG. 7. Same as Fig. 6, except for wind stresses. Arrows indicate wind stress directions.

However, there are significant differences among them (Figs. 10a and 11a). The NCEP LHF appears to agree with that of GSSTF2 within ~10 W m^{-2}, except for a negative bias of −20 W m^{-2} in the 40°–60°S band. The LHF of da Silva is smaller than that of GSSTF2 but with a difference of <10 W m^{-2}, except for the equatorial region (larger with the difference up to ~20 W m^{-2}) and the Southern Ocean (smaller by 20–40 W m^{-2}). The HOAPS has the lowest LHF in the Tropics among the four flux products. Compared to GSSTF2, the HOAPS LHF is smaller by 20–50 W m^{-2} in the Tropics. The discrepancy in the LHF among GSSTF2, HOAPS, and da Silva is primarily caused by the differences in the input parameters, as the moisture transfer coefficients used are very close. However, this situation is not true for NCEP. The moisture transfer coefficient of NCEP is significantly larger than that of GSSTF2 (and the other two flux datasets; Zeng et al. 1998), which

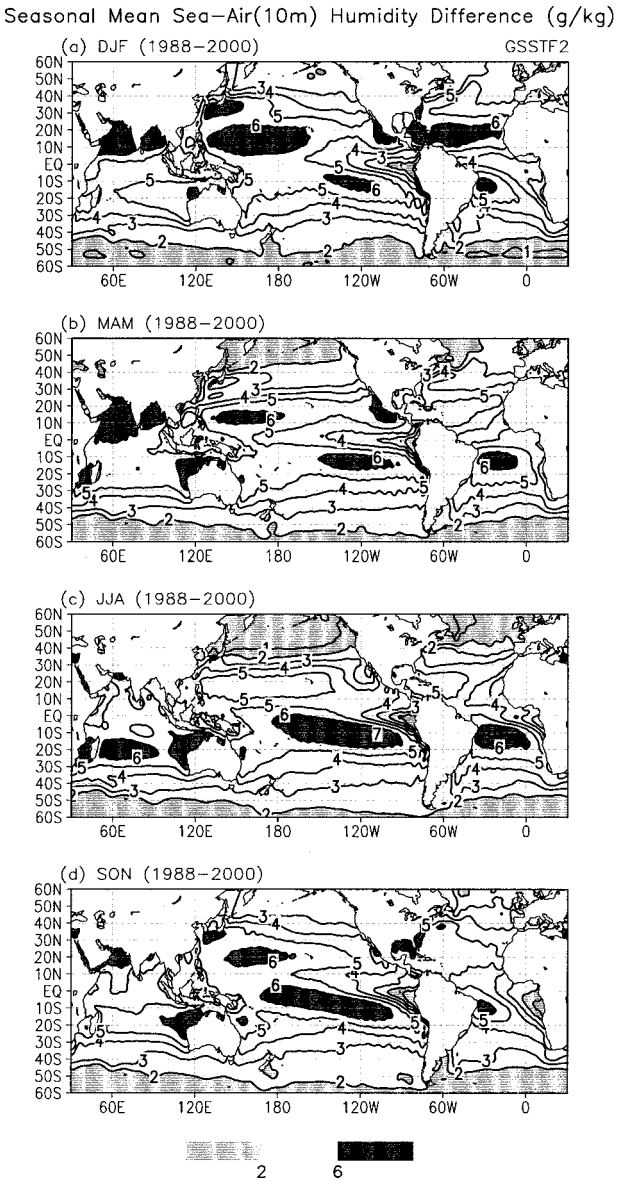

FIG. 8. Same as Fig. 6, except for sea–10-m humidity differences.

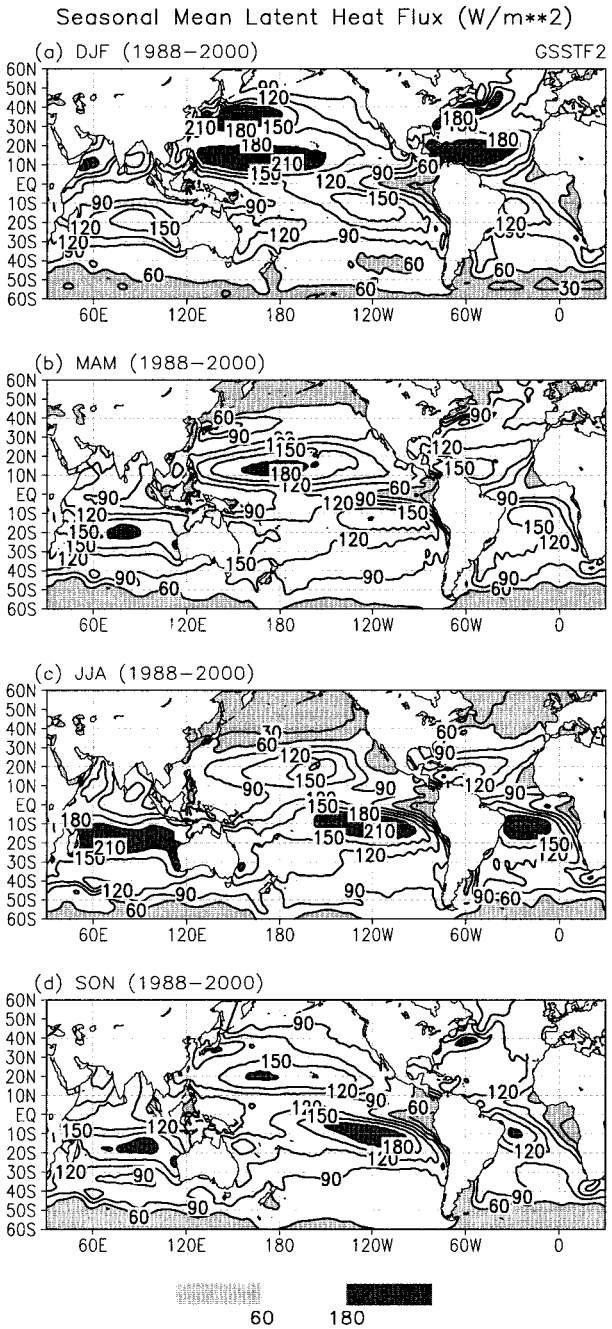

FIG. 9. Same as Fig. 6, except for LHFs.

appears to offset the effects of weaker winds and the smaller sea–air humidity difference on the LHF (Figs. 10 and 11). Thus, the LHF of NCEP and GSSTF2 appear to generally be in good agreement.

Figure 10b shows that $U_{10m,}$ for the four datasets, has a minimum at the equator and increases poleward, with the primary (secondary) maximum near 50° (in the trade wind belts) of both hemispheres. However, the NCEP U_{10m} is weaker with the difference reaching 1.2 m s^{-1} in the 40°S–40°N region but is stronger with the difference up to 0.5 m s^{-1} poleward of 40°, when compared with GSSTF2 (Fig. 11b). The HOAPS U_{10m} is also weaker in the Tropics of 30°S–30°N (the difference up to 1.5 m s^{-1}) but is stronger in the extratropics (the difference up to 1.5 m s^{-1}), as compared to GSSTF2. The da Silva U_{10m} is generally within 0.5 m s^{-1} of GSSTF2, except is higher by ~1 m s^{-1} near 20°N and is stronger by 1–2.5 m s^{-1} in the 40°–60°N band.

The Wentz (1997) SSM/I U_{10m} from 1987 to 1997 have been extensively evaluated with those of the Tropical Atmosphere–Ocean (TAO) and National Data Buoy Center (NDBC) buoys by Mears et al. (2001), and those of the ECMWF analysis and NCEP by Meissner et al. (2001). Meissner et al. (2001) pointed out that both global analyses did not assimilate the Wentz wind prod-

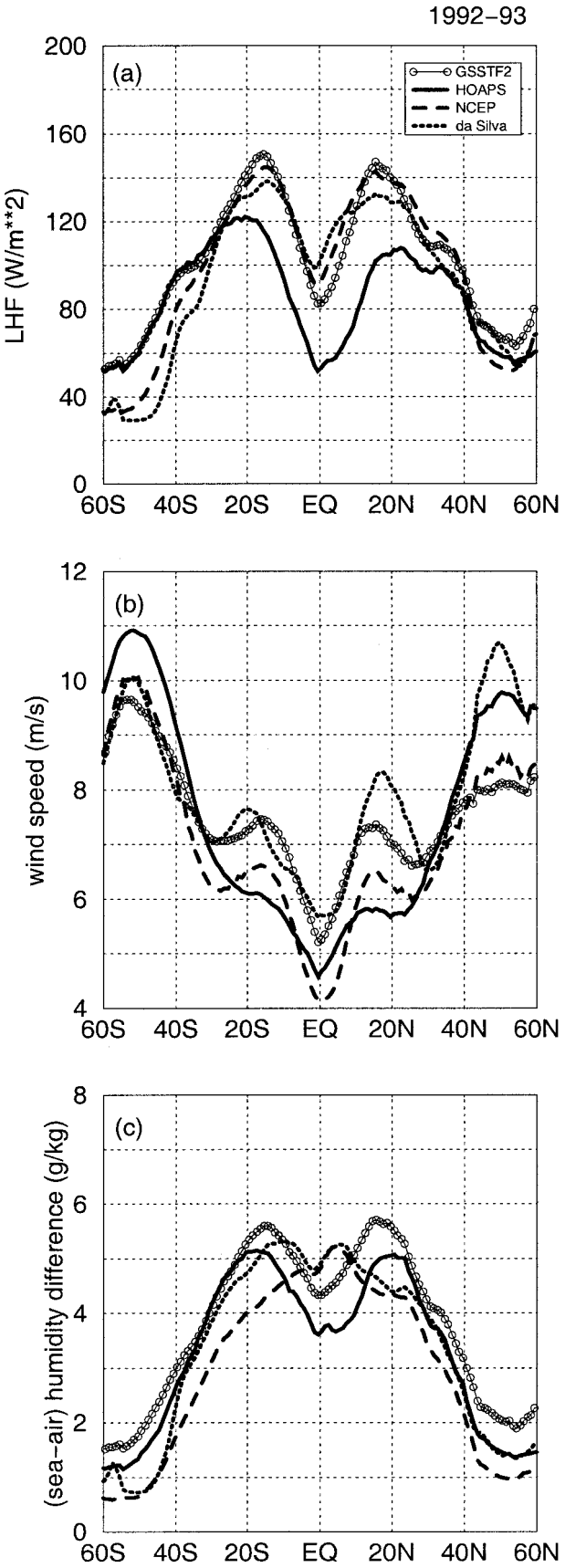

ucts and that the SSM/I wind speeds incorporated in NCEP were derived using a neural network algorithm and were different from those of Wentz (1997). Mears et al. (2001) found that the mean difference between SSM/I and buoy winds was typically <0.4 m s^{-1} and the SD error was <1.4 m s^{-1}. Meissner et al. (2001) found that the collocated SSM/I and NCEP U_{10m} had an SD difference of 2.4 m s^{-1}, which reduced to 1.2 m s^{-1} for the monthly averages, and that the NCEP U_{10m} was underestimated in the tropical Pacific and tropical Atlantic. Wang and McPhaden (2001) found the NCEP surface winds were weaker than those of TAO buoys by $\sim$1–1.5 m s^{-1} in the tropical Pacific. Smith et al. (2001) found the NCEP U_{10m} was underestimated by 0.4–1.0 m s^{-1} for five geographic regions (the North Atlantic, South Atlantic, Southern Ocean, western Pacific, and Arabian Sea), as compared to those measured by research ships during the 1990–95 World Ocean Circulation Experiment. Renfrew et al. (2002) found that the NCEP U_{10m} was 0.4 m s^{-1} higher than those measured by the research ship over the Labrador Sea. These results are consistent with this study.

Da Silva et al. (1994) assumed an anemometer height of 20 m to the entire wind dataset measured by ship anemometers of COADS to derive a Beaufort equivalent scale for determining visual wind speeds, which depend on sea states. However, Kent and Taylor (1997) found that the true anemometer heights had large standard deviations with the means generally much higher than 20 m and increasing with time. For example, they found that the mean anemometer height was 35.2 (24.2 m) with a standard deviation of 8.4 (10.9 m) in midlatitudes of the North Pacific (North Atlantic) during 1990. An underestimation of anemometer height can cause unrealistic higher ship anemometer-measured (and visual) wind speeds, because the higher wind speeds measured at the higher anemometer heights are assigned to the assumed lower levels. For the same error of anemometer height, the stronger the wind, the larger the wind speed error. This can cause a larger discrepancy of wind speeds in the high-wind regions. This is likely to be the major reason that a large discrepancy of U_{10m} in the high-wind region of the northern high latitudes is found between da Silva and GSSTF2. These previous studies and Fig. 3a and Table 4 suggest that the GSSTF2 U_{10m} is more accurate and that the differences in U_{10m} shown in Figs. 10b and 11b are caused primarily by the errors in HOAPS, NCEP, and da Silva.

Figure 10c shows that the sea–air humidity difference ($Q_s - Q_a$) is higher in the Tropics and decreases poleward. However, the meridional profiles of $Q_s - Q_a$ are

←

FIG. 10. Zonal averages of (a) LHF (b) 10-m wind speeds, and (c) sea–air humidity differences over global oceans during 1992–93 for GSSTF2, HOAPS, NCEP, and da Silva. Only the collocated monthly valid data from all four datasets are used.

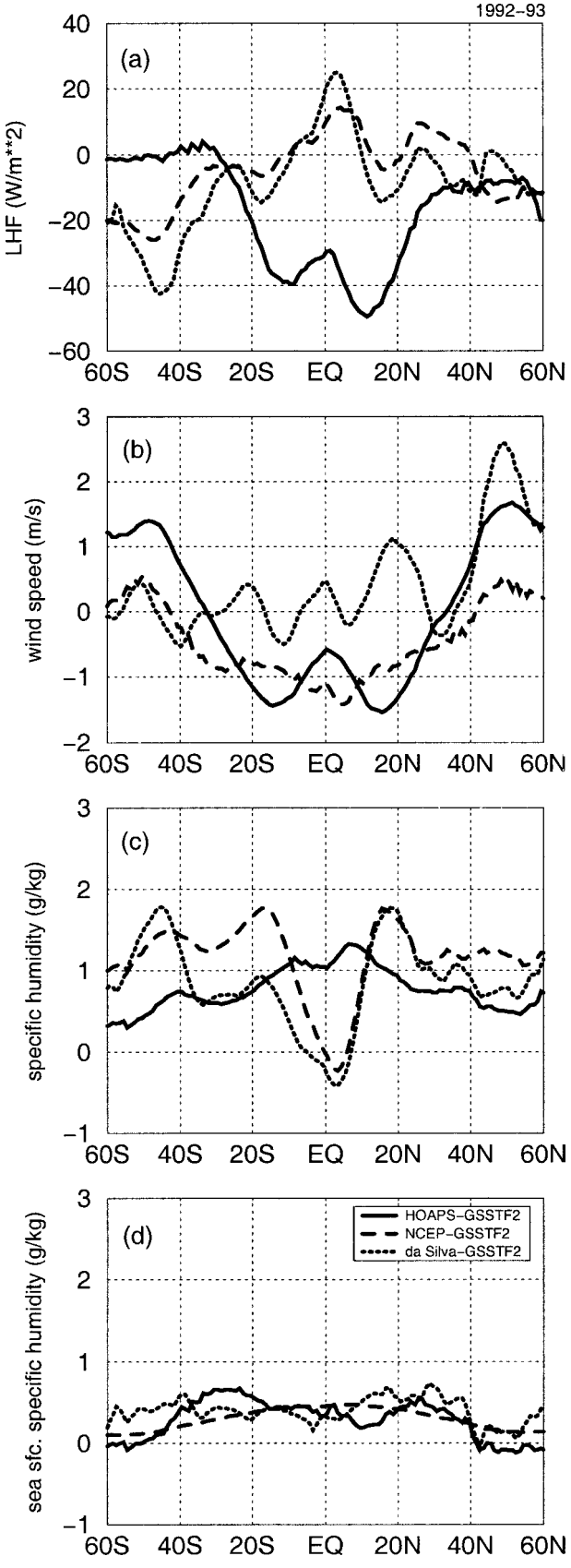

quite different in the Tropics among the four products. The $Q_s - Q_a$ of GSSTF2 and HOAPS has the maximum in the trade wind regions and decreases equatorward and poleward, while that of NCEP and da Silva generally has the maximum near the equator and decreases poleward. The discrepancy in $Q_s - Q_a$ is mainly due to the difference in Q_a. This can be clearly seen from Figs. 11c and 11d, which show the differences in Q_a and Q_s for the four datasets, respectively. The GSSTF2 has the smallest Q_s. However, the differences in Q_s among the four datasets are generally very small (<0.5 g kg^{-1}), which arise from the differences in the SST, sea level pressure, and formula for computing Q_s. Figure 11c shows that the NCEP 2-m Q_a is wetter than the GSSTF2 10-m Q_a by $\sim$1–1.7 g kg^{-1} in the regions poleward of $\sim$10°, with decreased differences near the equator. The 20-m Q_a of da Silva is wetter than the GSSTF2 10-m Q_a by $\sim$0.5–1.7 g kg^{-1} in the regions poleward of $\sim$10°, with small differences (<0.5 g kg^{-1}) near the equator. The HOAPS 10-m Q_a is wetter than the GSSTF2 10-m Q_a by $\sim$0.4–1.3 g kg^{-1}, with significant differences of 1–1.3 g kg^{-1} within $\sim$15° of the equator.

Since there is no ground truth for the global surface air humidity, we analyze the humidity discrepancies based on Table 4, Fig. 3b, and previous studies. Table 4 shows that the GSSTF2 Q_a has a positive bias of $\sim$1 ($\sim$0.7) g kg^{-1} in the tropical oceans (for the nine experiments over the tropical and midlatitude oceans). Figure 3b shows that the GSSTF2 Q_a has a positive bias for the moist region with Q_a of $\sim$16–20 g kg^{-1} but has a small negative bias for the dry region with Q_a of $\sim$3–6 g kg^{-1}. Wang and McPhaden (2001), Smith et al. (2001), and Renfrew et al. (2002) found that the NCEP surface air humidity had positive biases when compared with those measured by TAO buoys and research ships. Their results and this study imply that the GSSTF2–NCEP humidity difference shown in Fig. 11c is mostly due to the moist bias of NCEP. Previous studies (e.g., da Silva et al. 1994; Chou et al. 1997; Josey et al. 1999) found that ship observations overestimated dewpoint temperatures (by $\sim$0.5°C), which resulted in moist bias of the surface air humidity for COADS, and thus for da Silva. Their results and this study suggest that the GSSTF2–da Silva humidity difference shown in Fig. 11c is mostly due to the moist bias of da Silva. The results also suggest that the HOAPS Q_a is significantly overestimated in the tropical oceans, as it is larger than the moist biased Q_a of GSSTF2. These analyses suggest that the GSSTF2 Q_a is likely to be closest to the reality

←

FIG. 11. Zonal averages of differences of HOAPS, NCEP, and da Silva from GSSTF2 for (a) LHFs, (b) 10-m wind speeds, (c) surface air specific humidity, and (d) surface saturation specific humidity over global oceans during 1992–93. Only the collocated monthly valid data from all four datasets are used.

TABLE 5. Regional-mean LHF, 10-m wind speeds (U_{10m}), surface air specific humidity (Q_a), surface saturation specific humidity (Q_s), and sea–air humidity differences ($Q_s - Q_a$) over global oceans during 1992–93 for GSSTF2, HOAPS, NCEP, and da Silva.

Variable	Source	60°S–60°N	20°–60°N	20°S–20°N	20°–60°S
LHF	GSSTF2	108.2	104.1	122.1	94.3
(W m^{-2})	HOAPS	88.5	89.8	84.7	92.3
	NCEP	104.8	104.6	125.1	81.1
	Da Silva	99.7	98.8	123.4	72.5
U_{10m}	GSSTF2	7.4	7.3	6.6	8.3
(m s^{-1})	HOAPS	7.1	7.6	5.5	8.7
	NCEP	6.8	7.1	5.6	8.0
	Da Silva	7.6	8.1	6.8	8.3
Q_a	GSSTF2	12.1	10.2	16.6	7.8
(g kg^{-1})	HOAPS	12.9	10.9	17.7	8.4
	NCEP	13.2	11.4	17.5	9.2
	Da Silva	12.9	11.2	17.1	8.9
Q_s	GSSTF2	16.2	14.0	21.7	11.0
(g kg^{-1})	HOAPS	16.6	14.3	22.1	11.4
	NCEP	16.6	14.3	22.2	11.2
	Da Silva	16.6	14.5	22.1	11.4
$Q_s - Q_a$	GSSTF2	4.1	3.8	5.1	3.2
(g kg^{-1})	HOAPS	3.7	3.4	4.4	3.0
	NCEP	3.3	2.9	4.6	2.1
	Da Silva	3.7	3.2	5.0	2.6

among the four datasets analyzed, although it is still subject to regional biases.

Table 5 compares the regional averages of LHF and input parameters for the global oceans (60°S–60°N), northern extratropical oceans (20°–60°N), tropical oceans (20°S–20°N), and southern extratropical oceans (20°–60°S) during 1992–93 among GSSTF2, HOAPS, NCEP, and da Silva. The global-mean LHF is the largest for GSSTF2 (108.2 W m^{-2}) and the smallest for HOAPS (88.5 W m^{-2}), with a difference of 20 W m^{-2}. Over the tropical oceans, the HOAPS LHF has the maximum difference (37 W m^{-2}) from that of GSSTF2, whereas the other two datasets are comparable. This is mainly a result of weaker winds (weaker by ~1 m s^{-1}) coupling with smaller sea–air humidity difference (smaller by ~0.7 g kg^{-1}). The significant overestimation (wetter than GSSTF2 by 1.1 g kg^{-1}) of the surface air humidity in the tropical oceans is primarily the cause for the latter. The global-mean LHF of NCEP is comparable to that of GSSTF2, but the sea–air humidity difference and surface wind are weaker (by 0.8 g kg^{-1} and 0.6 m s^{-1}), which appear to offset the larger moisture transfer coefficient (Zeng et al. 1998). The LHF of da Silva is generally comparable to that of GSSTF2, except for the southern extratropical oceans. Over the southern extratropical oceans, the LHF of da Silva is the smallest among the four datasets, with a negative bias of 22 W m^{-2} as compared to GSSTF2. This discrepancy is most likely due to the errors arising from the interpretation of missing data in the large data-void southern extratropical oceans. In short, our analyses suggest that the GSSTF2 LHF, surface air humidity, and winds are likely to be more realistic than the other four datasets analyzed, although those of GSSTF2 are still subject to regional biases. More high-quality observations over global oceans are needed to do a more detailed regional validation and to confirm our conclusions.

7. Concluding remarks

The GSSTF2 is a 13.5-yr (July 1987–December 2000) global dataset of daily ocean surface turbulent fluxes of momentum, latent heat, and sensible heat, with 1° spatial resolution. Turbulent fluxes are derived from the surface winds (Wentz 1997) and surface air humidity (Chou et al. 1995, 1997) retrieved from SSM/I, as well as the SST and 2-m air temperature of the NCEP–NCAR reanalysis, based on the method of Chou et al. (1997) with two improvements (the von Kármán constant and salinity effect for Q_s). The directions of wind stress are taken from those of the surface winds, which are derived from a blend of the SSM/I wind speeds (Wentz 1997), surface wind vectors from ships, buoys, and NCEP–NCAR reanalysis following the method of Atlas et al. (1996).

Hourly fluxes computed from the ship data using the GSSTF2 bulk flux model validate well against those of 10 field experiments conducted by the NOAA/ETL (Fairall et al. 1996b, 1997, 2003) over the tropical and midlatitude oceans during 1991–99. Compared to the 10 experiments, the computed hourly wind stress has a negative bias of −0.0005 N m^{-2}, a SD error of 0.0106 N m^{-2}, and a correlation of 0.98. The computed hourly LHF has a bias of 4.5 W m^{-2}, a SD error of 19.6 W m^{-2}, and a correlation of 0.91. The computed hourly SHF has a negative bias of −0.2 W m^{-2}, an SD error of 7.3 W m^{-2}, and a correlation of 0.82. The computed SHF appears to have lower accuracy, as compared to the computed wind stress and LHF. This is most likely due to the fact that the small SHF is more sensitive to measurement and parameterization errors, especially the

diurnal variation of the cool skin effect. Overall the results suggest that the GSSTF2 flux model is generally accurate for weak and moderate winds, but slightly underestimates LHF and SHF for strong winds. This study suggests that the roughness lengths need to be improved for high winds.

The GSSTF2 daily wind stress, LHF, wind speed, surface air humidity, and SST compare reasonably well with those collocated with nine field experiments. Compared to the nine field experiments, the GSSTF2 daily wind stress has a positive bias of 0.0129 N m^{-2}, a SD error of 0.0774 N m^{-2}, and a correlation of 0.72. The daily LHF has a bias of 0.8 W m^{-2}, a SD error of 35.8 W m^{-2}, and a correlation of 0.83. The daily SHF has a positive bias of 6.4 W m^{-2}, a SD error of 10.1 W m^{-2}, and a correlation of 0.84. The daily surface wind speed has a bias of 0.36 m s^{-1}, a SD error of 1.38 m s^{-1}, and a correlation of 0.92. The daily surface air specific humidity has a bias of 0.67 g kg^{-1}, a SD error of 1.23 g kg^{-1}, and a correlation of 0.97. The daily surface air temperature has a negative bias of −0.47°C, a SD error of 0.82°C, and a correlation of 0.99. The daily SST has a negligible bias of 0.04°C, a SD error of 0.51°C, and a correlation of 1.0. In addition, the global distributions of 1988–2000 annual- and seasonal-mean turbulent fluxes show reasonable patterns related to the atmospheric general circulation and seasonal variations.

Zonal averages of LHF and input parameters over global oceans during 1992–93 are compared among the GSSTF1, GSSTF2, HOAPS, NCEP–NCAR reanalysis, and da Silva et al. (1994). Our analyses suggest that the GSSTF2 LHF, surface air humidity, and winds are likely to be more realistic than the other four flux products examined, although those of GSSTF2 are still subject to regional biases. More high-quality observations over the global oceans are vital to do a more detailed regional validation, to improve satellite retrieval, and to further confirm our conclusions. The GSSTF2 derived from the SSM/I is useful for climate studies and is available online at http://daac.gsfc.nasa.gov/CAMPAIGN_DOCS/hydrology/hd_gsstf2.0.html. We plan to produce a 0.25° dataset of surface turbulent fluxes over the global ocean using the newly improved version-5 SSM/I data of Wentz with a new bulk flux scheme with additional improvement for the high-wind conditions. The new dataset will be used for pixel validation of fluxes and input parameters.

Acknowledgments. This study was supported by the TRMM Program and Physical Oceanography Program, NASA/Office of Earth Science. The first author is especially grateful to R. Kakar, the TRMM Program Manager, and R. Adler, the TRMM Project Scientist, for their continuous support and encouragement. The SSM/I version-4 data of total precipitable water, wind speeds, and antenna temperatures produced by F. Wentz's group were obtained online at http://www.ssmi.com. The NCEP–NCAR reanalysis data were obtained from the NOAA–CIRES Climate Diagnostics Center online at http://www.cdc.noaa.gov/. The flux data of the NOAA/ETL research ships processed by C. Fairall's group were obtained from the SEAFLUX Web site at http://paos.colorado.edu/~curryja/ocean/. The HOAPS data were obtained from http://www.mpimet.mpg.de/Depts/Physik/HOAPS/. The COADS turbulent fluxes were provided by A. da Silva. Consultation related to the computer codes of the Wentz SSM/I antenna temperatures was provided by G. J. Huffman. The GSSTF1 and GSSTF2 are archived online at http://daac.gsfc.nasa.gov/CAMPAIGN_DOCS/hydrology/hd_gsstf2.0.html through the help of L. Chiu and W. L. Teng. Helpful comments on the original manuscript from two anonymous reviewers are greatly appreciated.

REFERENCES

Atlas, R., R. N. Hoffman, S. C. Bloom, J. C. Jusem, and J. Ardizzone, 1996: A multiyear global surface wind velocity dataset using SSM/I wind observations. *Bull. Amer. Meteor. Soc.,* **77,** 869–882.

Bourassa, M. A., D. G. Vincent, and W. L. Wood, 1999: A flux parameterization including the effects of capillary waves and sea state. *J. Atmos. Sci.,* **56,** 1123–1139.

Brunke, M. A., C. W. Fairall, X. Zeng, L. Eymard, and J. A. Curry, 2003: Which bulk aerodynamic algorithms are least problematic in computing ocean surface turbulent fluxes? *J. Climate,* **16,** 619–635.

Businger, J. A., J. C. Wyngaard, Y. Izumi, and E. F. Bradley, 1971: Flux profile relationships in the atmospheric surface layer. *J. Atmos. Sci.,* **28,** 181–189.

Charnock, H., 1955: Wind stress on a water surface. *Quart. J. Roy. Meteor. Soc.,* **81,** 639–640.

Chou, S.-H., 1993: A comparison of airborne eddy correlation and bulk aerodynamic methods for ocean–air turbulent fluxes during cold-air outbreaks. *Bound.-Layer Meteor.,* **64,** 75–100.

——, and M. P. Ferguson, 1991: Heat fluxes and roll circulations over the western Gulf Stream during an intense cold-air outbreak. *Bound.-Layer Meteor.,* **55,** 255–281.

——, R. M. Atlas, C.-L. Shie, and J. Ardizzone, 1995: Estimates of surface humidity and latent heat fluxes over oceans from SSM/I data. *Mon. Wea. Rev.,* **123,** 2405–2425.

——, C.-L. Shie, R. M. Atlas, and J. Ardizzone, 1997: Air–sea fluxes retrieved from Special Sensor Microwave Imager data. *J. Geophys. Res.,* **102,** 12 705–12 726.

——, W. Zhao, and M.-D. Chou, 2000: Surface heat budgets and sea surface temperature in the Pacific warm pool during TOGA COARE. *J. Climate,* **13,** 634–649.

Clayson, C. A., C. W. Fairall, and J. A. Curry, 1996: Evaluation of turbulent fluxes at the ocean surface using surface renewal theory. *J. Geophys. Res.,* **101,** 28 503–28 513.

Curry, J. A., and Coauthors, 1999: High-resolution satellite-derived dataset of the surface fluxes of heat, freshwater, and momentum for the TOGA COARE IOP. *Bull. Amer. Meteor. Soc.,* **80,** 2059–2080.

——, and Coauthors, 2003: SEAFLUX. *Bull. Amer. Meteor. Soc.,* submitted.

da Silva, A., C. C. Young, and S. Levitus, 1994: *Algorithms and Procedures.* Vol. 1, *Atlas of Surface Marine Data 1994,* NOAA Atlas NESDIS 6, 83 pp.

Esbensen, S. K., D. B. Chelton, D. Vickers, and J. Sun, 1993: An analysis of errors in Special Sensor Microwave Imager evaporation estimates over the global oceans. *J. Geophys. Res.,* **98** (C4), 7081–7101.

Fairall, C. W., E. F. Bradley, J. S. Godfrey, J. B. Edson, G. S. Young,

and G. A. Wick, 1996a: Cool-skin and warm-layer effects on sea surface temperature. *J. Geophys. Res.*, **101,** 1295–1308.

——, ——, D. P. Rogers, J. B. Edson, and G. S. Young, 1996b: Bulk parameterization of air–sea fluxes for Tropical Ocean Global Atmosphere Coupled Ocean–Atmosphere Response Experiment. *J. Geophys. Res.*, **101** (C2), 3747–3764.

——, A. B. White, J. B. Edson, and J. E. Hare, 1997: Integrated shipboard measurements of the marine boundary layer. *J. Atmos. Oceanic Technol.,* **14,** 338–359.

——, E. F. Bradley, J. E. Hare, A. A. Grachev, and J. B. Edson, 2003: Bulk parameterization of air–sea fluxes: Updates and verification for the COARE algorithm. *J. Climate,* **16,** 571–591.

Garratt, J. R., 1977: Review of drag coefficients over oceans and continents. *Mon. Wea. Rev.*, **105,** 915–929.

Hellerman, S., and M. Rosenstein, 1983: Normal monthly wind stress over the world ocean with error estimates. *J. Phys. Oceanogr.*, **13,** 1093–1104.

Josey, S. A., E. C. Kent, and P. K. Taylor, 1999: New insights into the ocean heat budget closure problem from analysis of the SOC air–sea flux climatology. *J. Climate,* **12,** 2856–2880.

Kalnay, E., and Coauthors, 1996: The NCEP/NCAR 40-Year Reanalysis Project. *Bull. Amer. Meteor. Soc.,* **77,** 437–471.

Kent, E. C., and P. K. Taylor, 1997: Choice of a Beaufort equivalent scale. *J. Atmos. Oceanic Technol.,* **14,** 228–242.

Kubota, M., K. Ichikawa, N. Iwasaka, S. Kizu, M. Konda, and K. Kutsuwada, 2002: Japanese Ocean Flux Data Sets with Use of Remote Sensing Observations (J-OFURO). *J. Oceanogr.,* **58,** 213–215.

——, A. Kano, H. Muramatsu, and H. Tomita, 2003: Intercomparison of various surface latent heat flux fields. *J. Climate,* **16,** 670–678.

Large, W. G., and S. Pond, 1982: Sensible and latent heat flux measurements over the ocean. *J. Phys. Oceanogr.*, **12,** 464–482.

Liu, W. T., K. B. Katsaros, and J. A. Businger, 1979: Bulk parameterization of air-sea exchanges of heat and water vapor including the molecular constraints at the interface. *J. Atmos. Sci.,* **36,** 1722–1735.

Mears, C. A., D. Smith, and F. J. Wentz, 2001: Comparison of Special Sensor Microwave Imager and buoy-measured wind speeds from 1987 to 1997. *J. Geophys. Res.,* **106,** 11 719–11 729.

Meissner, T., D. Smith, and F. J. Wentz, 2001: A 10-year intercomparison between collocated SSM/I oceanic surface wind speed retrievals and global analyses. *J. Geophys. Res.,* **106,** 11 731–11 742.

Oost, W. A., G. J. Komen, C. M. J. Jacobs, and C. van Oort, 2002: New evidence for a relation between wind stress and wave age from measurements during ASGAMAGE. *Bound.-Layer Meteor.,* **103,** 409–438.

Renfrew, I. A., G. W. K. Moore, P. S. Guest, and K. Bumke, 2002: A comparison of surface layer and surface turbulent flux observations over the Labrador Sea with ECMWF analyses and NCEP reanalyses. *J. Phys. Oceanogr.,* **32,** 383–400.

Reynolds, R. W., and T. S. Smith, 1994: Improved global sea surface temperature analyses. *J. Climate,* **7,** 929–948.

Schulz, J., P. Schluessel, and H. Grassl, 1993: Water vapor in the atmospheric boundary layer over oceans from SSM/I measurements. *Int. J. Remote Sens.,* **14,** 2773–2789.

——, J. Meywerk, S. Ewald, and P. Schluessel, 1997: Evaluation of satellite-derived latent heat fluxes. *J. Climate,* **10,** 2782–2795.

Smith, S. R., D. M. Legler, and K. V. Verzone, 2001: Quantifying uncertainties in NCEP reanalyses using high-quality research vessel observations. *J. Climate,* **14,** 4062–4072.

Taylor, P. K., and M. A. Yelland, 2001: The dependence of sea surface roughness on the height and steepness of the waves. *J. Phys. Oceanogr.,* **31,** 572–590.

Wagner, D., E. Ruprecht, and C. Simmer, 1990: A combination of microwave observations from satellites and EOF analysis to retrieve vertical humidity profiles over the ocean. *J. Appl. Meteor.*, **29,** 1142–1157.

Wang, W., and M. J. McPhaden, 2001: What is the mean seasonal cycle of surface heat flux in the equatorial Pacific? *J. Geophys. Res.,* **106,** 837–857.

Webster, P., C. A. Clayson, and J. A. Curry, 1996: Clouds, radiation, and the diurnal cycle of sea surface temperature in the tropical western Pacific. *J. Climate,* **9,** 1712–1730.

Weller, R. A., and S. P. Anderson, 1996: Surface meteorology and air-sea fluxes in the western equatorial Pacific warm pool during the TOGA Coupled Ocean–Atmosphere Response Experiment. *J. Climate,* **9,** 1959–1990.

Wentz, F. J., 1997: A well calibrated ocean algorithm for SSM/I. *J. Geophys. Res.,* **102,** 8703–8718.

Wick, G. A., W. J. Emery, and L. H. Kantha, 1996: The behavior of the bulk-skin sea surface temperature difference under varying wind speed and heat flux. *J. Phys. Oceanogr.,* **26,** 1969–1988.

Woodruff, S. D., S. J. Lubker, K. Wolter, S. J. Worley, and J. D. Elm, 1993: Comprehensive Ocean–Atmosphere Data Set (COADS) release la: 1980–92. *Earth Syst. Monitor,* **4,** 4–8.

Yelland, M., and P. K. Taylor, 1996: Wind stress measurements from the open ocean. *J. Phys. Oceanogr.,* **26,** 541–558.

——, B. I. Moat, P. K. Taylor, R. W. Pascal, J. Hutching, and V. C. Cornell, 1998: Wind stress measurements from the open ocean corrected for airflow distortion by the ship. *J. Phys. Oceanogr.,* **28,** 1511–1526.

Zeng, X., M. Zhao, and R. E. Dickinson, 1998: Intercomparison of bulk aerodynamic algorithms for the computation of sea surface fluxes using TOGA COARE and TAO data. *J. Climate,* **11,** 2628–2644.